THERMAL PROTECTION OF
REENTRY VEHICLES BY ACTIVELY COOLED NOSETIPS

R. E. Walker*

J. W. Hidahl**

ABSTRACT

This paper presents recent analytical modeling efforts and clear-air ground test results of a transpiration-cooled nosetip (TCNT) design. The discrete water injection platelet TCNT described was conceived and created by the Aerojet Liquid Rocket Company to achieve the performance requirements for severe reentry vehicle trajectories. Nosetip ground test data are presented from the Air Force Systems Command's Arnold Engineering Development Center (AEDC) hyperballistic Track G test facility in varying clear-air environments. Thermal performance computer modeling techniques, combining both local heat blockage and boundary layer recovery enthalpy reduction are outlined.

INTRODUCTION

During the last several years test programs and analyses have been conducted to define the mechanisms and limits involved in using a liquid coolant (water) to provide thermal protection for reentry vehicle nose cones. Impetus for the work was the need to increase the reliability of the reentry vehicle under conditions of high aeroheating and adverse weather encounter. ᵀⁿ the last two years much progress has been made in understanding the mechanisms and defining operating limits involved in cooling nosetips. The purpose of this paper is to document the current status of the work. Although advancements have been made in both the aeroheating and weather survivability areas, this paper deals with the aeroheating thermal protection aspects of the work.

Although primarily related to reentry nose cones the aeroheating thermal protection of reentry vehicles has application to many problems of current interest, both for military and civilian use, such as:

1.   Leading edge coolant for shuttle type reentries to increase reliability and perhaps reduce weight.

2.   Leading edge cooling of evader type powered aircraft.

3.   Use in wake seeding and/or electronic attenuation/clarification application.

* Senior Engineering Specialist, Aerojet Liquid Rocket Company
**Senior Engineer, Aerojet Services Company

4. The use in high speed weapons intercept or attack systems.

Most of the recent pertinent test data were from tests conducted in the hypervelocity range at Air Force Systems Command's Arnold Engineering Development Center (AEDC). From July 1978 through July 1979 twenty five tests were conducted in the 1000 foot long test cell "G" with launch velocities in the range of 16,000 to 18,000 feet per second and at cell pressures of 100 to 500 mm Hg, equivalent to altitudes of 47,000 to 11,000 feet. Of these 25 tests, 10 were in clear air and 15 were through varying ice field densities. For the clear air tests considered, the nosetip coolant flow rates and distributions over the nosetip surface were the primary variables. Data acquisition consisted of inflight coolant flow rate and surface temperature measurements and inflight laser photographs of the nosetip surface. In addition, post test inspections of the test piece were used to define overall nosetip surface conditions.

NOMENCLATURE

A	=	$h_1/(G\ Cp\ T)$
B	=	$h_1/(K\ T)$
C	-	Diffusion coefficient
C_D	=	Drag Coefficient
	-	Slot equivalent
		Blowing ratio, $(\rho V)_c/(\rho V)_e$
	=	Mass flow rate
	=	Liquid side film coefficient
K	=	Conductivity
M	=	Mach Number
Nu	=	Heat transfer Nussult Number
Nu	=	Mass Transfer Nussult Number
P	-	Pressure
net	-	Net heat flux to surface of fin
	=	Total heat to droplet
		Mean droplet radius
	-	Droplet Reynolds Number, $2\ r_m\ (V_e-V_c)\ \rho_g$
	-	Liquid Reynolds Number in coolant slot, $V_c\ \rho_c$
	-	$-A/2 + \sqrt{A^2/4 + B}$
	-	Schmidt Number
	=	Stanton Number
T	=	Temperature
	=	Time
	=	Velocity
	=	Vaporization rate
	-	Weber Number, $V_e^2\ \rho_e/\rho$

	=	Density
	=	Surface Tension
	--	Viscosity

SUBSCRIPTS

	-	Coolant property
		Droplet property
		Edge property
		Surface property
		Gas property
		Vapor property
		Without blowing

NOSETIP CONFIGURATION

The ten clear air tests in the AEDC Track G hypersonic facility were conducted during performance of the Advanced Ballistic Reentry Program (ABRV) (Reference (1)) using nosetips of one basic design; although internal coolant flow metering differences were designed into the nosetips.

All the nosetips tested were hemispherical (R_N = 0.65 inches), with base half angles of approximately 17° (overall length = 0.5 inches) The nosetips were fabricated from thin sheets (.0007 to .002 inch) of 347 stainless steel which were diffusion bonded to form a monolithic structure with the mechanical properties of the parent material. The flow passages needed for flow metering and surface distribution were chemically etched in the individual sheets or platelets prior to diffusion bonding. Coolant flow distribution over the nosetip surface was characterized by collecting and measuring the flow rate from 15 independent hydraulic sections which were aligned axially down the nosetip. The surface of the nosetips was cooled by approximately 4400 individual coolant exit slots which occupied approximately one half of the nosetip surface area. Flow metering within tne nosetip was tailored to provide different coolant distributions for specific thermal prctection applications.

A photograph of the nosetip external configuration is shown on Figure 1. Typical flow metering paths within the nosetip are shown on Figure 2. It is this in-depth flow metering which allowed the surface coolant distribution to be tailored to provide test data over a range of local coolant mass fluxes. Coolant distributions for three of the tested nosetips are shown on Figure 3.

TRACK OPERATING CONDITIONS AND INSTRUMENTATION

The independent track operating parameters were the nosetip launch velocity, pressure and temperature within the 1000 foot long cell. Detailed descriptions of the Track G facility are contained in Reference (2). For the series of clear air nosetip tests under consideration the launch velocities were 17 to 17.5 KFPS while cell pressure produced altitudes equivalent to 11,000 to 20,000 feet. These conditions provided excellent simulation of actual reentry environments. The resulting heat flux distributions over the nosetip for the range of test conditions are shown on Figure 4. Cell temperature was near ambient, 539°R, for all tests and the resulting enthalpy ranged from 6500 Btu/lbm at range entrance to 3800 Btu/lbm at range exit. The velocity degradation with flight distance accounts for most of this variation.

A major factor in the success of the test series was the data acquisition available at the facility. The data consisted of coolant flow rate measurements, nosetip surface temperature plots, and laser photographs. Coolant total flow rates were calculated from x-ray photographs of the displacement of the piston in the coolant cylinder. A drawing of the nosetip and model holder containing the coolant system is shown on Figure 5. When coupled with the nosetip hydraulic data and design computer code the total coolant flow rate could be used to accurately determine the coolant mass flux distribution

within approximately 5%. A photograph of the nosetip in flight near the mid-range location is shown on Figure 6. The coolant water droplets and nosetip surface pattern may be seen on the photograph.

Thermal mapping of the nosetip surface was accomplished through the use of image converter cameras. Two systems were used, one with a temperature range of 2250°R to 8100°R and the other with a range of 2850°R to 8100°R. Measurement uncertainty for both systems is approximately ± 200°R. The maximum measurable temperature for either system in these tests was defined by the nosetip material melt temperature (3000°R). The main limitation to the otherwise excellent data system was the rather high lower limit on temperature sensitivity. The nosetip design temperature was 2260°R, only 10°R higher than the lower sensitivity limit of the best IC camera. Consequently, a large amount of valuable thermal information was not available for analysis. Improvements in the temperature sensitivity range appear possible in the near future.

NOSETIP OPERATING CONDITIONS AND DATA TRENDS

The data contained in Table I summarize the nosetip and track operating conditions for the 10 clear-air tests. Thermal data from these tests were available at up to 4 stations on each test. However, at some stations, temperatures were below the IC camera sensing levels, and on some tests, shock cap or after-body flare masked the data. There was sufficient data from the first test series, however, to allow the data to be used to design the coolant distribution flow profile for the second test series. A plot of these data along with the design mass flux profiles is shown on Figure 7.

Although the data available from the two test series was not complete enough to provide a solid basis for a comprehensive empirical model, it did provide an excellent base from which to correlate the engineering analytical model. This basic model formulation was supported by both the thermal data trends and the appearance of the liquid coolant mantle surrounding the nosetip which was observed from the inflight laser photographs. Before proceeding to the description of the analytical model some additional comments relating to the empirically observed nosetip behavior will be discussed.

The most interesting of these observations, and perhaps the most unexpected, is the apparent "self healing" aspect of the thermal protection phenomena associated with stagnation point blunting and "dimpling". The blunting is caused by melting and/or erosion as the nosetip stagnation region approached the material melt temperature.

The concave depression or "dimple" has been a characteristic of all nosetip testing performed in the facility. The dimpling is slight, 10 to 30 mils deep and 30 to 50 mils in diameter. However, it appears that this dimpling constitutes a significant self-healing aspect of the nosetip. Since the stagnation point has generally been undercooled, either by design or through fabrication anomalies, it has tended to get hot. This results in melting and/or increased erosion. The formation of the dimple is a natural protective occurrence which reduces local heating and establishes an equilibrium between delivered and required coolant flow rates. The data

334

presented on Figure 8 show the influence of stagnation point mass flux on observed surface temperature. These data show a substantial decrease in coolant required for a given surface temperature as dimpli g occurs.

A second observation of significance is the apparent insensitivity of coolant requirements to nosetip roughness. An untested nosetip has an effective surface roughness estimated to be approximately 5 mils. After repeated tests, particularly in a weather environment, the roughness approaches 25 to 30 mils. No differences have been found in the coolant flow/surface temperature relationship for the two cases. It should be noted that the smooth wall boundary layer momentum thickness at the base of the nosetip is typically on the order of 1.5-2.0 mils.

A third observation, which led to the formulation of the coolant vaporization modeling improvements, was the presence of a mantle of liquid droplets surrounding the nosetip during flight. Coupled with this observation is the fact that the nosetip cooling models which existed at the time the test program was initiated considered only the influences of local coolant injection and could not adequately predict the observed thermal behavior (low surface temperature) in the downstream portions of the nosetip. These observations from the first test series led to the development of the present downstream cooling model which uses coolant droplet atomization, drag and vaporization to predict distributed thermal energy exchange in the nosetip boundary layer.

NOSETIP MODELING TECHNIQUE

The objective of this work was to establish analytical procedures for predicting the performance of the Aerojet discrete injection cooled nosetip. These procedures considered not only the local blockage and internal heat transfer phenomena but also the influences of coolant carryover from upstream injection slots. In addition to the development of the analytical model, an initial calibration of the model using existing test data was accomplished.

The current Aerojet nosetip concept utilizes film cooling as a major means of protection against reentry heating. The coolant, which is injected from discrete slots as a mixture of liquid and vapor, provides protection through two mechanisms. Some local heat transfer blockage, caused by local injection, occurs just downstream of each slot. Also, as the heated injected liquid is entrained in the boundary layer and flows along the surface of the body, it absorbs energy directly from the hot gases and vaporizes, thereby cooling the downstream region. This process also alters the boundary layer development compared to that for a non-blowing surface.

Analysis procedures which have been developed in the past have only included local effects. No upstream injection cooling has been considered. This overly conservative approach has resulted in unrealistically high predicted coolant requirements. Also, the previous model did not allow accurate predictions of the coolant requirements in the downstream region of the nosetip and, thus, was of little value in designing a flight experiment where accurate predictions of surface temperatures over the entire tip are desirable.

335

Considerable experimental data has been recently obtained on the ABRV program. These data indicate that the downstream cooling effects are a significant contributor to total nosetip coolant requirements, and may reduce coolant requirements by as much as 50 percent. This data provided an excellent base for the initial formulation of a downstream cooling model; however more detailed data are desirable to better model the individual downstream cooling and blockage phenomena.
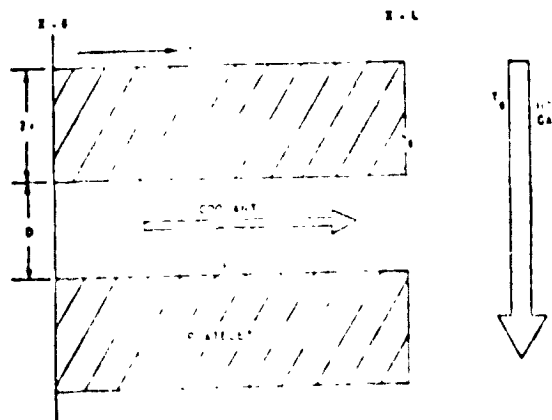
ANALYTICAL MODEL DESCRIPTION

The nosetip aerodynamic environment is characterized using the ABRES Shape Change Code (ASCC). Included in the code are the influences of surface roughness ard heat flux augmentation at the stagnation point. This code generates the baseline non-blowing heat flux and pressure distributions and the boundary layer thickness and edge properties. Relevant data are put on mass storage data files for use by the downstream cooling and design codes. Coolant atomization, vaporization and boundary layer enthalpy reduction are calculated within the downstream cooling program to provide a reduced surface heat flux distribution. The program uses this reduced heat flux together with the pressure and enthalpy distribution, the nosetip hydraulic input and the particle environment (if any) to compute surface heating and erosion.

The heat transfer mechanisms which influence nosetip performance predictions and coolant requirements, i.e., the internal heat transfer, the local boundary layer heat blockage, and the downstream cooling will be discussed in more detail in the following paragraphs.

Internal Heat Transfer

A schematic diagram of the thermal model for the internal nosetip cooling is shown below. The nosetip surface is considered to be composed of platelets which form fins which are "2t" thick and having coolant channels between which are "D" deep. The coolant enters the channels at X=0 at a temperature T_{co} and at a rate G per unit cooled wall surface area. At the end of the platelets, X=L, the platelets are exposed to a hot gas at temperature T_g with a surface film coefficient h_g.

336

It is assumed that the heat conduction in the platelets is one-dimensional and that the platelet material and coolant properties are not temperature dependent.

The resulting form of the fin equation as used in the internal cooling model (Reference (3)) is:

$$T_w = T_{co} + Q_{net}/(K\ r_1) \tag{i}$$

Mass Transfer Blockage

Two mass transfer blockage models were examined during the ABRV Program. Originally, a correlation based on the work of Bartle and Leadon, Reference 4, was used. However, during the analyses of the ground test results, the model was found to yield much lower stagnation point temperatures than were measured. A blockage correlation based on the work done on the Nosetip Cooling Technology Program (NCT), Reference 5, was found to yield better correlation with the test data.

A comparison of the blockage ratios, q/q_o, predicted by the two models is shown on Figure 9 as a function of the blowing parameter, B'. The forms of the two correlations are similar. The Bartle and Leadon model is based on a correlation which relates the blockage ratio, q/q_o, to the mainstream specific heat ratios C_p^*, the blowing ratio, F, and the unblown Staton number, ST_o:

$$q/q_o = \frac{\dfrac{FC_p^*}{ST_o}}{\left[1 + F\ \dfrac{C_p^*}{3\ ST_o}\right]^3 - 1} \tag{2}$$

The NCT model relates the blockage to these same parameters but takes the form

$$q/q_o = \frac{1}{(1 + FM\ \dfrac{C_p^*}{St_o}\ F)^3} \tag{3}$$

Where FM characterizes the blockage as a function of land position. FM takes the form:

$$FM = .03 + .14\ e^{-2.8\ X/L} \tag{4}$$

Where X/L is the relative land position.

Downstream Cooling Model

The analyses of the test data gathered on the ABRV Program, as well as test data presented on previous programs, have indicated the need to include

337

downstream cooling effects in the nosetip analytical model. Initial formulation and development of this model was completed during the ABRV Program. In addition some correlation of the model with the existing test data was accomplished. As more of the recent test data are evaluated and the empirical trends are identified, these data will be used to further refine the model.

The downstream cooling model was formulated based on boundary layer energy balance considerations. The enthalpy in the boundary layer is reduced as a result of vaporization of coolant injected upstream. The phenomena considered include droplet atomization, acceleration, heat transfer, mass transfer and boundary layer thermal dilution. Equations relating to these processes were based on the work of Ingebo (Reference (6)) and Priem (Reference (7)) and may be found in the Appendix. These processes are shown schematically on Figure 10. The coolant is atomized at the slot exit and enters the gas stream as a series of droplets. The droplets are accelerated by the gas stream and vaporized as they proceed downstream. The vaporizing droplets exchange energy with the boundary layer gases resulting in a reduced boundary layer enthalpy. In addition, the coolant injection changes the boundary layer temperature and velocity profiles compared to the non-blowing case.

COPRELATION OF MODEL WITH TEST DATA

Nosetip surface temperature measurements resulting from the two test series were used to correlate the engineering analytical model. Preliminary correlation results of the new model are displayed in Figure 11 as solid lines for four tests. The measured temperature data are indicated on the plot by the circle-line combination. The dashed lines demonstrate the previous model (no downstream cooling influence) predictions for the same test conditions. As can be seen from the figures, the current revised model results in an improved predictive capability at body angles of greater than 20°.

Improvements in the stagnation region modeling which will include an improved modeling cf stagnation region heat flux and inclusion of the affects of blunting and dimpling are currently being evaluated.

CONCLUSIONS

Based on the test program and subsequent analytical model development several conclusions have been drawn. These include:

1. Excellent test data were obtained from 10 clear air tests at flight environmental conditions during two test series. Data from the first test series were used to design the coolant flow distribution for test series 2 and data from both series were used to develop and provide initial calibration for a nosetip cooling model.

2. The nosetip cooling model provides predictions of coolant requirements which significantly improved accuracy compared to previous models. The model includes characteristics of the three cooling mechanisms.

Internal cooling has been modeled using a fin equation with constant heat transfer coefficient. Local boundary layer blockage is computed using a correlation derived from tests which were expressly designed to provide blockage data for discrete injection nosetips. The downstream cooling routine considers atomization of the injected coolant; acceleration of the droplets; drop vaporization and mixing of the vapor with the boundary layer gas; and the reduction in boundary layer enthalpy and heat transfer which results from this mixing.

3. Good correlation to the clear air track test data was obtained using the analytical model.

4. Further model development and verification testing to better define the various cooling mechanisms involved in downstream cooling is justified and recommended. These tests should include:

(a) Cold flow tests to better characterize coolant penetration and atomization.

(b) Hot gas tests (T $\sim$ 1500°F) to characterize coolant vaporization.

(c) Aeroheating tests with instrumented nosetips in a plasma arc environment to provide the necessary nosetip temperature data for further model calibration.

REFERENCES

(1) "Advanced Ballistic Reentry Vehicle (ABRV) TCNT Development Program Final Report," Report 290770-004-001, ASC to AVCO-SD, April, 1980.

(2) Trimble, M.H., Smith, k.T. and Matthews, R.K., "AEDC High Temperature Testing Capabilities," AEDC-TR-78-3, April 1978.

(3) "ALRC - TCNT Subsystem ABRV, Phase II, Flight Test," Proposal No. LR 947768, ALRC to AVCO-SD, August, 1977.

(4) Bartle, R.E. and Leadon, B.M., "The Effectiveness as a Universal Measurement of Mass Transfer Cooling in a Turbulent Boundary Layer," Proceedings of the 1962 Heat Transfer and Fluid Mechanics Institute.

(5) Jaffe, N.A., et al., "Final Technical Report, Nosetip Cooling Technology (NCT) Program Investigation of Discrete Injection Cooling," Aerotherm Division/Acurex Corporation Technical Report. SAMSO TR 73-380, October, 1973.

(6) Ingebo, R.P. and Foster, N.H., "Drop Size Distribution for Cross Breakup of Liquid Tests in Airstreams," NASA TN 4087, October, 1957.

(7) Priem, R.J. and Heidmann, M.F., "Propellant Vaporization as a Design Criterion for Rocket Engine Combustion Chambers," NASA TR R-67, 1960.

TABLE i. AEDC TRACK G CLEAR AIR TESTS

Nosetip S/N	Test No.	Cell Press. (Torr)	Launch Vel. kfps	Range Entrance Stagnation Point Heat Flux,Btu/ft^2	Stag. Press. (psia)	Mid-Range Flow Rate Ratio	Max Temp. (^{o}R)	Loc.	Comments
Test Series No. 1:									
G-1	5046	350	17.7	24,700	2180	.69	3000	30°	Many Spots
G-1	5049	350	17.6	24,200	2160	.64	3000	0°-2°	Stag Pt Dimpled
G-1	5057	350	16.9	21,100	1990	.92	2400	0°-2°	-
G-2	5058	350	17.6	24,200	2160	.54	3000	0°-2°, 30°-35°	-
G-1	5060	350	17.6	24,200	2160	1.0/.2*	3000	0°-10°	Flow Leak
Test Series No. 2:									
G-4	5249	350	17.0	21,500	2010	.51	?	-	-
G-7	5252	_...	1 9	21,100	1990	.45	3000	0°-10°	-
G-7	'254	35	16.9	23,200	1990	.38	2880	0°-5°	-
G-7	5258	350	16.9	23,200	1990	.32	3000	15°-30°	-
G-5	5259	500	16.9	23,200	2830	.62	≤3000	0°-90°	-

*Actual fl rate through nosetip estimated to be this low due to massive coolant leak.
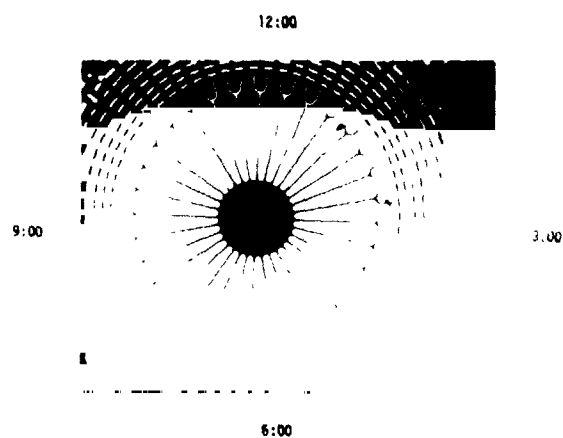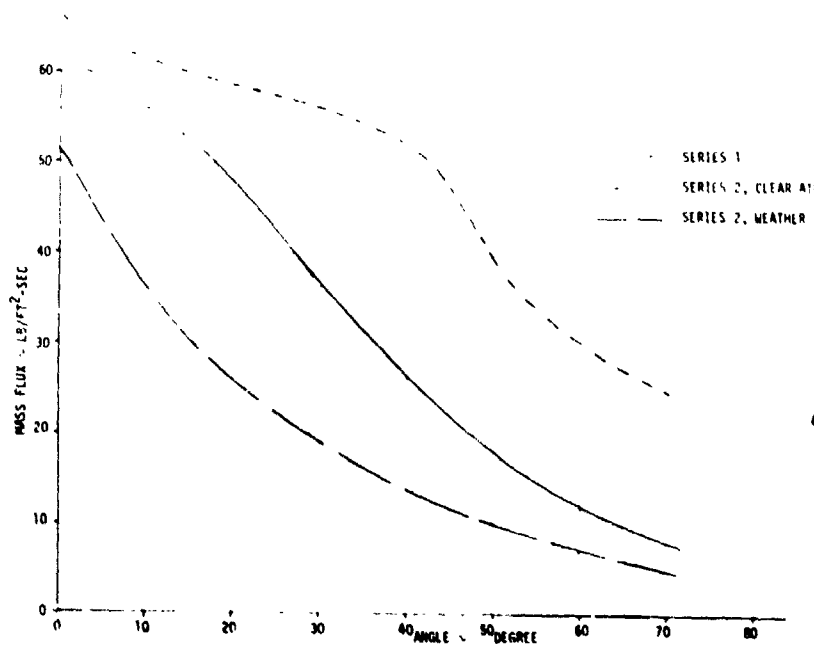
Figure I. AEROJET NOSETIP

Figure 2. TYPICAL METERING PLATELET

Figure 3. MASS FLUX DISTRIBUTION

TRACK G HEAT FLUX DISTRIBUTIONS (ASCC CODE,
R_n = 0.65 IN, SMOOTH WALL)

350 Torr Sta. 20 (Mid Range)

500 Torr, Sta 20 (Mid Range)

350 Torr, Sta 40 (Exit Station)
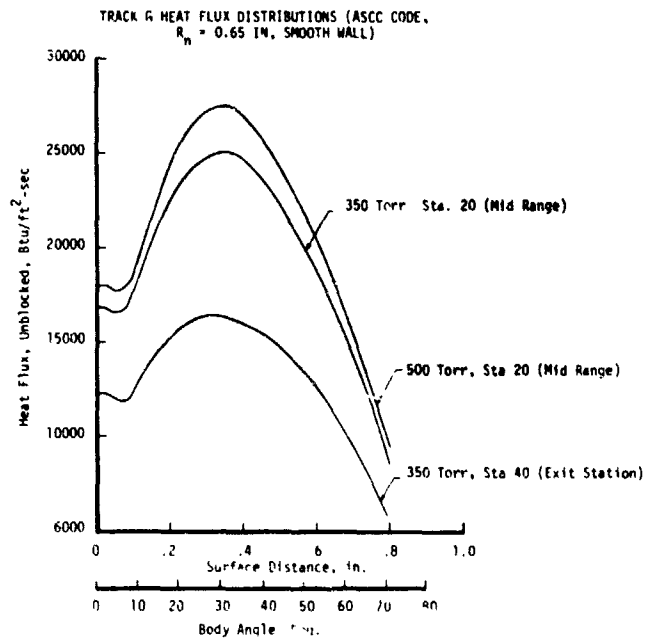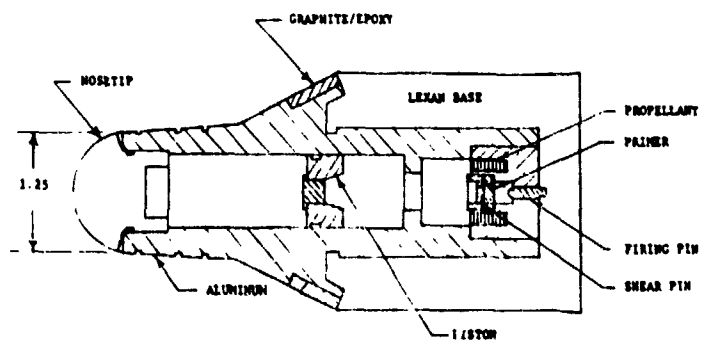
Figure 4.

Figure 5. NOSETIP AND MODEL HOLDER
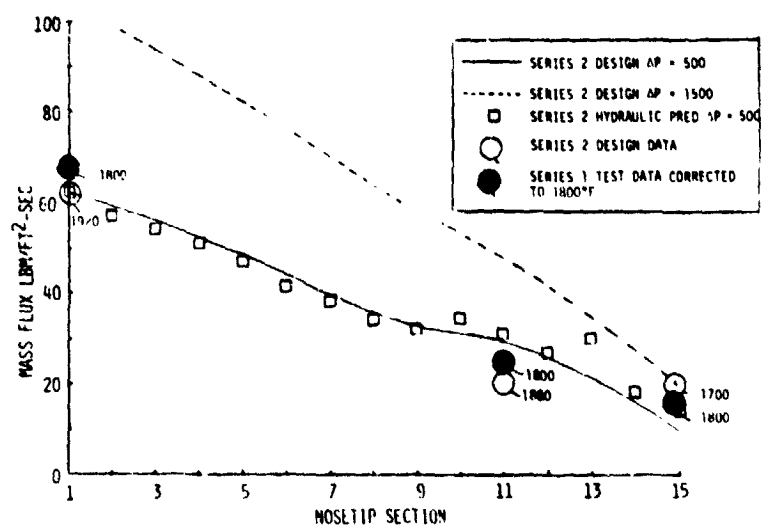
Figure 6.   NOSETIP IN FLIGHT

Figure 7.   COMPARISON OF SERIES 1 and 2
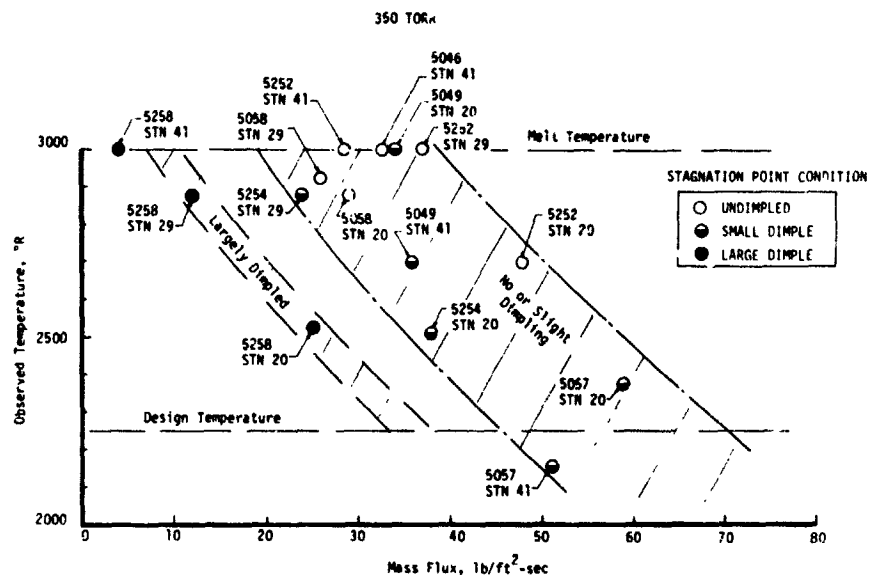   FLOW DISTRIBUTION WITH TEST DATA

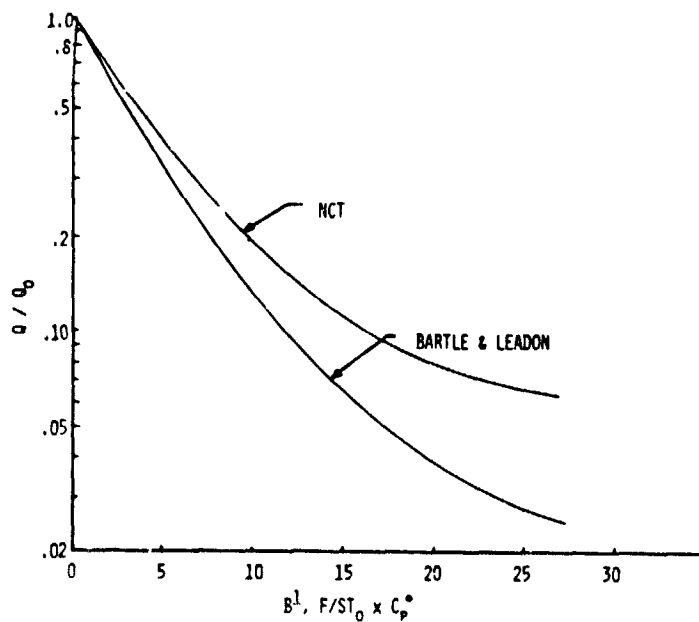Figure 8. TRACK G CLEAR AIR STAGNATION
POINT TEST DATA

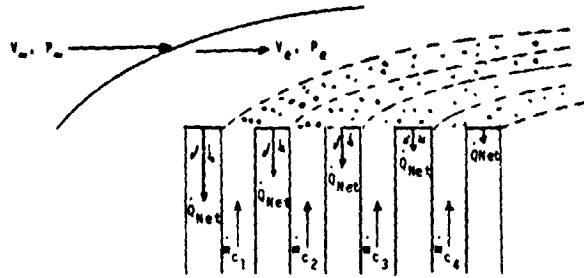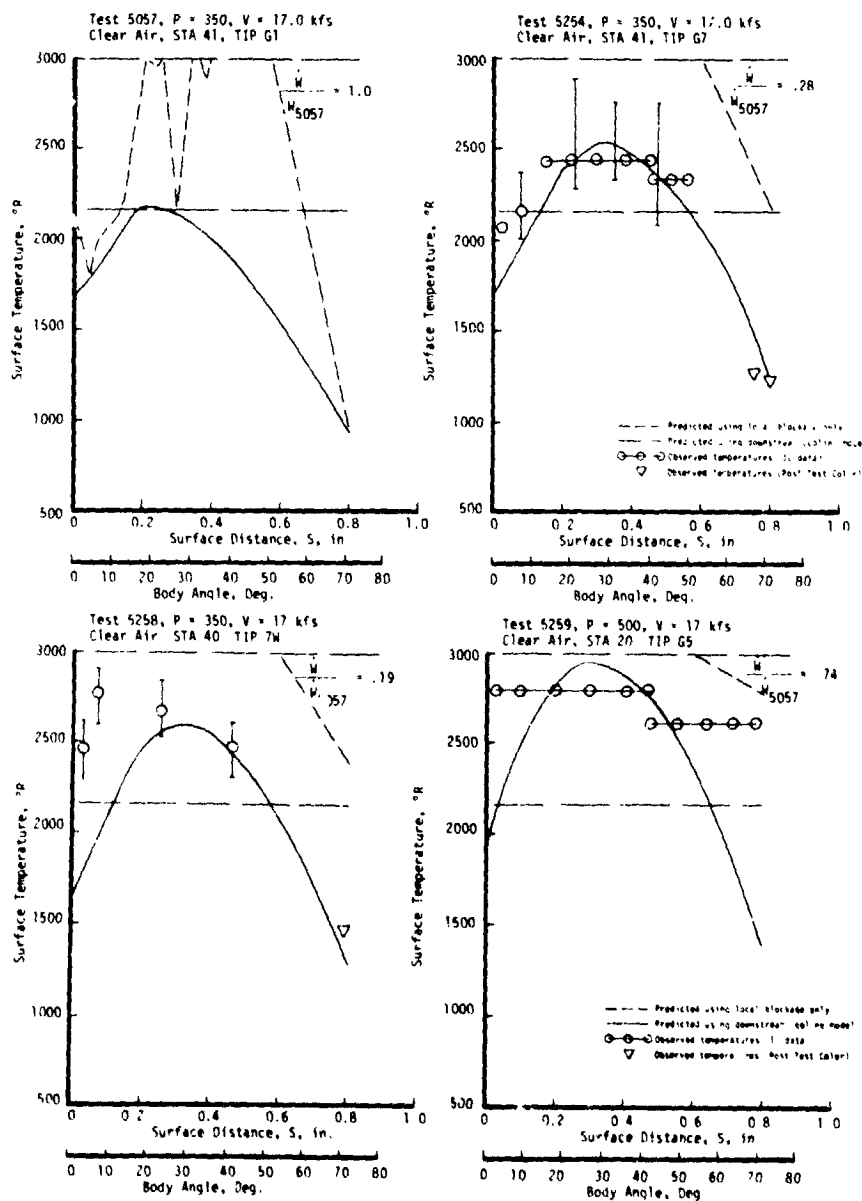
Figure 9. BLOCKAGE CORRELATION COMPARISONS

344

COOLANT ATOMIZATION AT SLOT EXIT $= f$ (SLOT DIM, $(\rho V)_c$, $(\rho V)_e$, COOLANT PROPERTIES)

COOLANT VAPORIZATION $= f$ (COOLANT PROPERTIES, GAS PROPERTIES, ΔV, DROP $_{DIA}$)

DROPLET/JET TRAJECTORY $= f$ ($(\rho V^2)_c$, $(\rho V^2)_e$, DROP $_{DIA}$)

ENTHALPY REDUCTION $= f$ (m VAPORIZED UPSTREAM)

HEAT FLUX REDUCTION $= f$ (ENTHALPY REDUCTION)

Figure 10.   DOWNSTREAM COOLING PROCESSES

Figure 11.   COMPARISON OF MODEL PREDICTIONS
WITH TRACK G DATA

345

APPENDIX

EQUATIONS USED IN DOWNSTREAM COOLING MODEL

I.   DROPLET ATOMIZATION (REFERENCE (6))

$$r_m = 1.95 \ (WE * REY * V_e/V_c)^{-0.25} \ D_o$$

II.   DROPLET DRAG/ACCELERATION (REFERENCE (7))

$$\frac{\Delta V_d}{\Delta t} = -0.375 \ C_D \ \frac{\rho_g}{\rho_c} \ \left[\frac{V_e - V_c}{r_m} \right]^2$$

$$C_D = 27 \ (R_e)^{-0.84} \qquad (M \leq 0.5)$$

$$C_D = f \ (M)* \qquad (M > 0.5)$$

III.   DROPLET HEAT TRANSFER

$$Q_D = 2 \ \Pi \ r_m \ K \ N_u \ (T_g - T_c) \ Z$$

$$N_u = 2 + .6 \ P_r^{.33} \ R_e^{.5}$$

$$Z = \frac{y}{e^{y-1}}$$

$$y = \frac{\dot{W}_v \ C_p}{2 \ K \ r_m \ N_u}$$

IV.   DROPLET MASS TRANSFER (REFERENCE (7))

$$W = \frac{2 \ \pi \ C \ MW_g \ r_m \ N_{um} \ P_v \ \alpha}{RT}$$

$$\alpha = P_s/P_v \ \ln \ (P_s/(P_s - P_v))$$

$$N_{um} = 2 + 0.6 \ S_c^{.33} \ R_e^{.5}$$

---

*From "Compressible Fluid Flow", by A. H. Shapiro, The Ronald Press Company, New York, 1953